CONF-9510212--21

LA-UR- 95-4003

Title: PERFORMANCE OF LONG-PULSE SOURCE REFERENCE TARGET-MODERATOR-REFLECTOR CONFIGURATIONS

Author(s): E. J. Pitcher, G. J. Russell, P. A. Seeger, P. D. Ferguson

Submitted to: ICANS XIII Conference, Villigen, Switzerland, 11-14 Oct 95

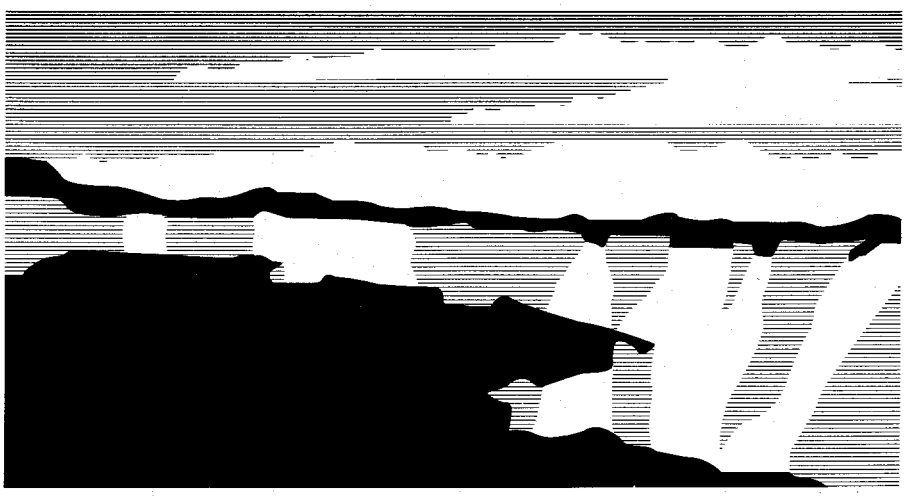

Los Alamos
NATIONAL LABORATORY

Form No. 836 R5
ST 2629 10/91

ICANS-XIII
13th Meeting of the International Collaboration on
Advanced Neutron Sources
October 11-14, 1995
Paul Scherrer Institut, 5232 Villigen PSI, Switzerland

PERFORMANCE OF LONG-PULSE SOURCE REFERENCE TARGET-MODERATOR-REFLECTOR CONFIGURATIONS

Eric J. Pitcher, Gary J. Russell, Philip A. Seeger, and Phillip D. Ferguson

Manuel Lujan, Jr. Neutron Scattering Center, Los Alamos National Laboratory, USA

ABSTRACT

We have calculated the performance of five similar target-moderator-reflector geometries that are reasonably well optimized for long-pulse source applications. For all cases, the moderators are fully coupled; that is, no poisons, decouplers, or liners are used. For each case, the energy- and time-dependent characteristics of the moderator source brightness have been parameterized using empirical functions. These parameterizations have been made available to users of the Monte Carlo neutron scattering instrument design code MCLIB for use in evaluating the performance of neutron scattering instruments on a long-pulse source.

1. Introduction

There is currently considerable debate within the neutron scattering community regarding the performance of certain classes of neutron scattering instruments on a "long-pulse" spallation source, that is, a neutron source fed by a proton beam whose pulse width is considerably longer than a few tens of microseconds. For proton beams with such pulse widths, the moderator pulse widths (or, more precisely, their full-widths at half-maximum) are governed by the proton pulse width rather than the storage time in the moderating media. As such, decoupling of the moderator does not lead to a reduction in the moderator pulse width and serves only to reduce the decay constant of the moderator pulse and, more significantly, reduce both the instantaneous and time-integrated source brightness [1].

Recently, the Monte Carlo-based neutron scattering instrument simulation code using the MCLIB library has been developed to such a state that it can now be used as a design tool [2]. The neutron source for this code is the leakage of neutrons from the moderator. Hence, one must provide the MCLIB source subroutine with a characterization of this leakage, both in time and in energy. We have performed this characterization for a reference coupled target system with five different reflector configurations.

Keywords: Coupled Moderator, Composite Reflector, Long-Pulse Source, MCLIB

2. Reference Target System Geometry

The reference geometry is a singly-split tungsten target with a square cross section. Horizontal and vertical cross sections along the proton beam axis are shown in Figure 1. The upper section of the target is $10 \times 10 \times 8.9$ cm^3, with a homogenized material composition equivalent to that of a clad rod target design capable of handling 1 MW of beam power (70.24 v% W, 18.66 v% Inconel-718, and 11.10 v% D_2O). The lower section has dimensions $12 \times 12 \times 23.1$ cm^3, and a homogenized material composition of 83.3 v% W and 16.7 v% D_2O. Both sections are completely enclosed in 0.2-cm-thick Inconel-718 target canisters. The flux trap gap between the two target sections is 14.6 cm high.

Surrounding the flux trap are four fully-coupled liquid-H_2 moderators, each 5 cm thick with a viewed surface area of 13×13 cm^2. The ortho/para-hydrogen fraction used in the calculation is 50/50 and the temperature is 20 K. Each moderator has wrapped about its perimeter a 1-cm-thick layer of H_2O, with a temperature of 293 K. The two surfaces of each moderator perpendicular to the neutron flight paths are covered by cryogenic moderator canisters, which, on each side of a moderator, are modeled as two 0.35-cm-thick plates of Aluminum-6061 separated by a 0.5-cm-thick vacuum gap. For each moderator, the distance from the proton beam centerline to the inner surface of liquid H_2 is 7.35 cm.

Before striking the target, the 800-MeV proton beam passes through a proton beam window, represented by two 0.108-cm-thick Inconel-718 plates separated by a 0.2-cm gap filled with H_2O. The proton beam profile is parabolic with a 7-cm circular diameter. The proton beam channel upstream of the target is 9 cm in diameter.

The total reflector size is fixed at 150 cm diameter by 150 cm high. The reflector composition and geometry were varied for the five reference cases reported here. In one case, the reflector has a single composition of 90 v% Be and 10 v% D_2O. For the other four cases, the reflector is

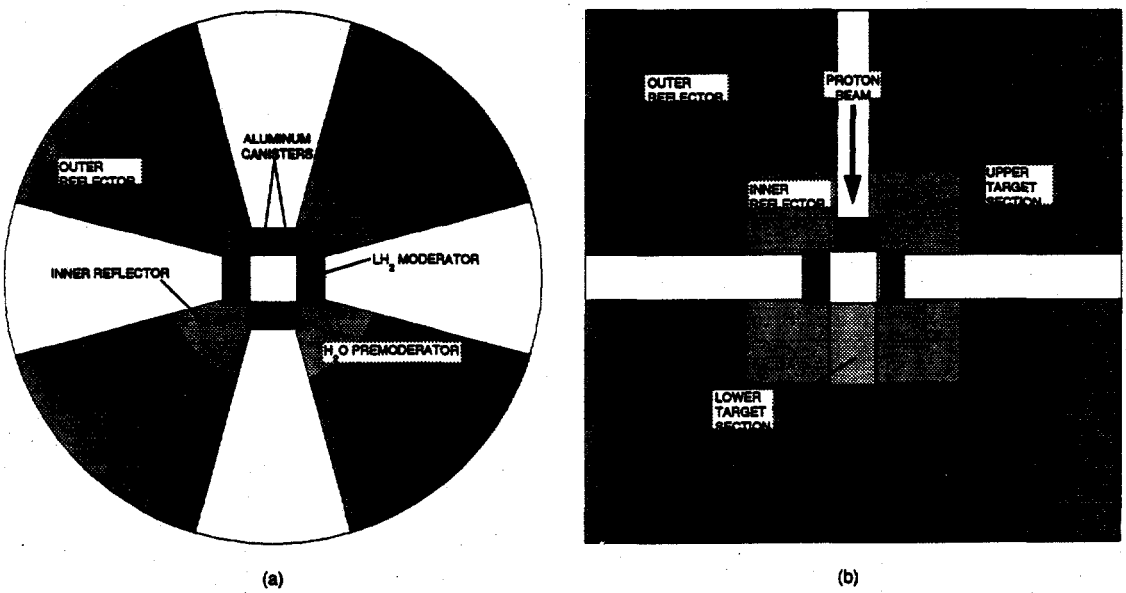

Figure 1. Cross-sectional views of the target station model. (a) Plan view, where the proton beam direction is perpendicular to the plane of the page; (b) Elevation view.

composite. The inner reflector is consistently 90 v% Be and 10 v% D_2O; for two cases the outer reflector is 90 v% Pb and 10 v% D_2O, while for the other two cases it is 90 v% Ni and 10 v% D_2O. For each outer reflector composition the inner reflector diameter and height were set to both 40 cm and 60 cm. These five reference reflector geometries are summarized in Table 1.

Table 1. Reflector characteristics for the five reference cases.

CASE	INNER REFLECTOR DIAMETER & HEIGHT (cm)	INNER REFLECTOR MATERIAL COMPOSITION	OUTER REFLECTOR MATERIAL COMPOSITION
40-cm Be/Ni	40	90 v% Be & 10 v% D_2O	90 v% Ni & 10 v% D_2O
60-cm Be/Ni	60	90 v% Be & 10 v% D_2O	90 v% Ni & 10 v% D_2O
40-cm Be/Pb	40	90 v% Be & 10 v% D_2O	90 v% Pb & 10 v% D_2O
60-cm Be/Pb	60	90 v% Be & 10 v% D_2O	90 v% Pb & 10 v% D_2O
150-cm Be	150	90 v% Be & 10 v% D_2O	n/a

3. Results

We used the LAHET Code System (LCS) to calculate the performance of each target-system geometry. The LCS is composed primarily of two Monte Carlo transport codes, LAHET and MCNP. LAHET is a model-based code that simulates the transport and interaction of high-energy nucleons, pions, and muons with stationary nuclei. The user may select from a variety of physics models [3] for simulating nuclear processes. For these calculations, we used the Bertini intranuclear cascade model, the GCCI level density model, the preequilibrium exciton model, the Dresner evaporation model, the Fermi breakup model, the RAL fission model, and neutron elastic scattering below 100 MeV. This combination of models shows good agreement with a broad range of experimentally-measured quantities [4]. MCNP is a data-based code that simulates the transport and nuclear interaction of neutrons with energies less than 20 MeV.

3.1 Energy Spectrum

The magnitude of the energy-dependent brightness is derived from point detector tallies placed 10 m from the moderator leakage surfaces. As all four moderators in the model are identical, the point detector tallies for all four moderators are averaged together in order to reduce the statistical error. Results for the five cases are shown in Figure 2. Also shown, for comparison, are the calculated results of Ageron [5] for the Cold Source 2 at the Institut Laue Langevin (ILL) in Grenoble, France, which is currently the world's most intense cold source. From Figure 2, it is evident that an all-beryllium reflector yields the highest time-integrated

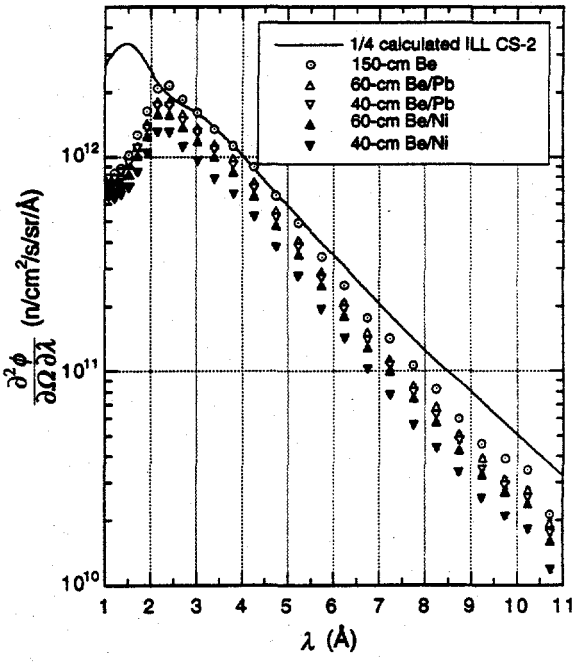

Figure 2. Brightness as a function of neutron wavelength λ for the five reference cases. For reference, the ILL CS2 spectrum at 1/4 power is also shown.

brightness at long wavelengths. Further, the Be-Pb composite provides a higher time-integrated brightness than does the Be-Ni composite. This is expected since Ni is a moderate neutron absorber and its presence should degrade the source brightness.

3.2 Time Spectrum

In addition, we calculated the time dependence of the source brightness by tallying neutrons crossing the moderator leakage surfaces. For the purpose of evaluating the temporal characteristics, we integrate the brightness from 0 to 5 meV (>4.04 Å), where the spectrum generally follows a linear dependence with energy. By setting the upper limit sufficiently low, we concentrate on the region of the spectrum that is typically most critical to optimize. Higher upper limits (e.g., 80 meV) could potentially lead to different conclusions about source performance. For example, the presence of an ambient premoderator and a sufficiently thin hydrogen moderator can significantly enhance the 20- to 80-meV region of the spectrum while it may have a detrimental effect on the 0 to 5-meV region.

Time-dependent pulse shapes for the five reference cases are shown in Figure 3 for an instantaneous proton pulse. From Figure 3(a), we see that the time-dependent peak brightness is the same to within 15% for all five reflector geometries. Note that the peak brightness for the 40-cm Be/Pb case is about 10% higher than for all other cases, which is a result of additional neutron production via spallation in the innermost portion of the outer Pb reflector. Figure 3(b) illustrates the decay constant. For reflector geometries with fast decays, a single decay constant fits the data well for times greater than about 300 μs. However, for geometries with appreciable tails, the decay is not a simple exponential and the value of the decay constant depends strongly on the time interval over which the fit is made.

Figure 4 shows the temporal response when the instantaneous pulses of Figure 3 are convolved with a 1-ms flat-top proton pulse. Here, three cases (150-cm Be, 60-cm Be/Pb, and 40-cm Be/Pb) exhibit nearly the same time-dependent peak brightness, while the 60-cm Be/Ni and 40-

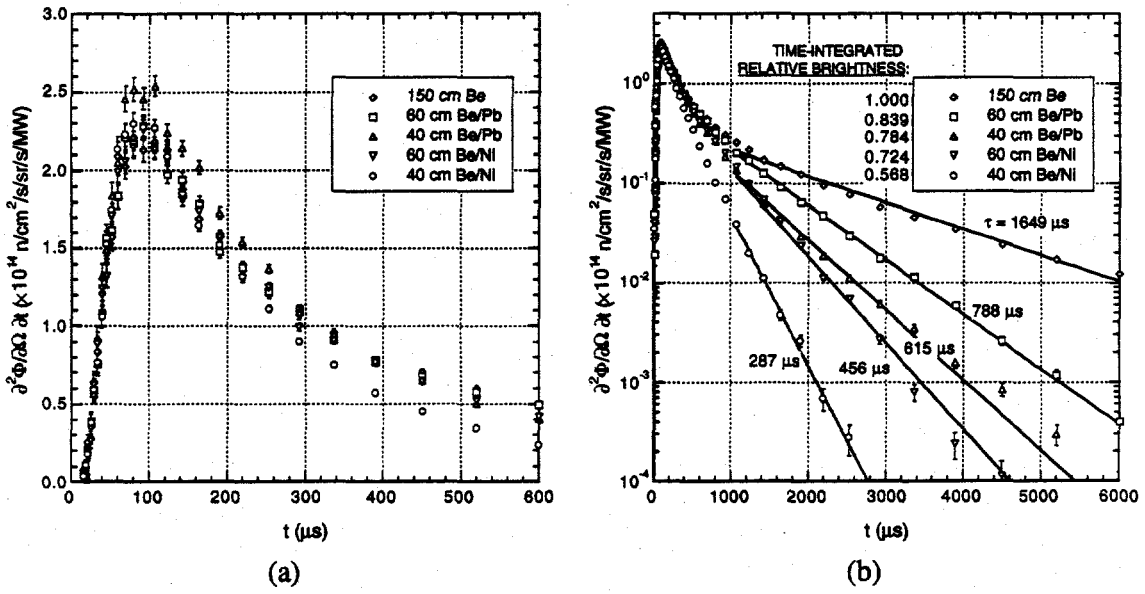

Figure 3. Instantaneous pulse shapes for neutrons with energy $E < 5$ meV for the five reference cases where the brightness is plotted on (a) a linear scale, and (b) a logarithmic scale.

cm Be/Ni are lower by about 7% and 23%, respectively. Note the effect of the decay constant on the brightness at 2 ms. For example, even though the 150-cm Be and 40-cm Be/Pb have nearly the same peak brightness, the 40-cm Be/Pb case is a factor of three lower in brightness at 2 ms. Depending on the application, this faster decay may prove to be a distinct advantage.

In Figure 5 we compare the temporal response of the source brightness for the 60-cm Be/Pb geometry for three cases: an instantaneous proton pulse, a 0.5-ms pulse, and a 1-ms pulse. The ratios of the time-dependent peak brightness is 3:1.6:1 for the instantaneous, 0.5-ms, and 1-ms pulses, respectively.

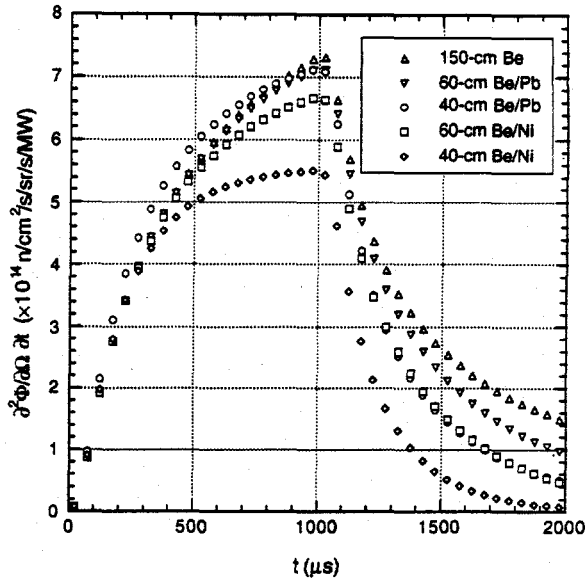

Figure 4. Pulse shapes (E < 5 meV) for a 1-ms proton pulse for the five reference cases.

3.3 Time-Energy Spectrum

A full characterization of the source brightness requires the calculation of the double differential of the source brightness in both time and energy. Tallying neutrons crossing the moderator leakage surfaces, we bin into 4 energy bins per decade from 178 μeV to 10 eV, and into 16 time bins per decade from 100 ns to 86.6 ms. An example of this detail is shown in Figure 6, which is a contour plot of source brightness as a function of time and energy for the 60-cm Be/Pb case. This detail is then used to evaluate the accuracy of source parameterization described in the next section.

3.4 Reduced Time Spectrum

In the slowing-down region, it is well known that the pulse shape is nearly invariant when the neutron leakage time t is normalized by the neutron wavelength λ. We take advantage of this fact when characterizing this region by tallying the neutrons crossing the moderator leakage surfaces as a function of the "reduced time" t/λ from 0.63 μs/Å to 100 μs/Å with a resolution of 20 bins per decade, and in coarse energy bins of one bin per decade from 1 meV to 1 keV. Results of this analysis are shown in Figure 7 for the 60-cm Be/Pb case. We see that the pulse shape when plotted as a function of reduced time is nearly the same for energies in the range 1 to 1000 eV.

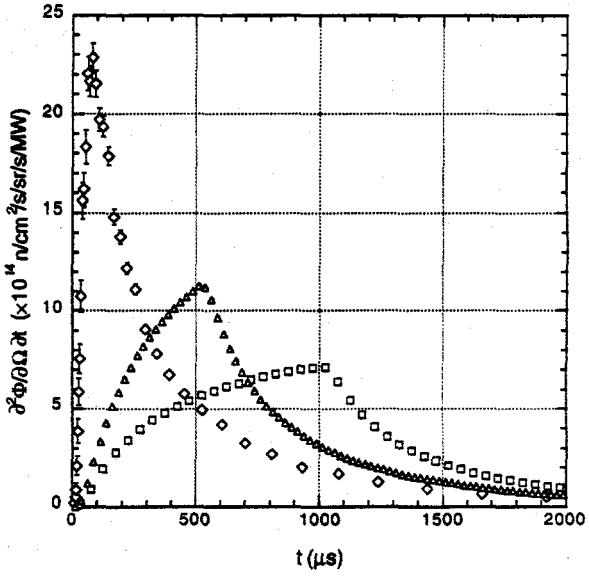

Figure 5. Pulse shapes (E < 5 meV) for the 60-cm Be/Pb case for three proton pulse widths: (◆) instantaneous; (▲) 0.5 ms; (■) 1 ms.

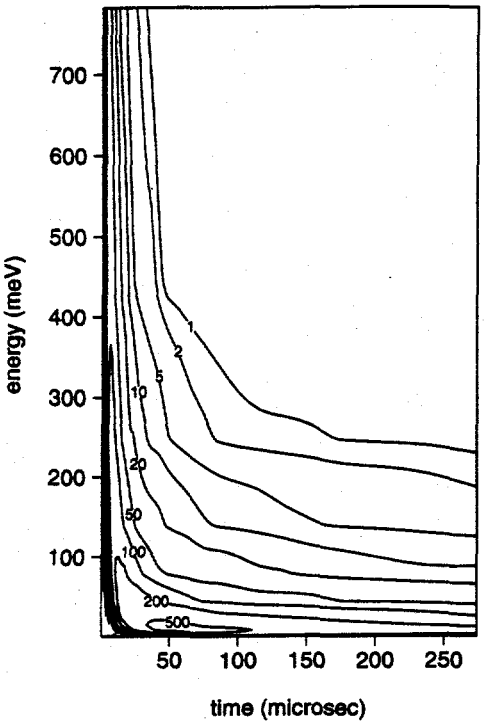

Figure 6. Contour plot of brightness as a function of time and energy for the 60-cm Be/Pb case. The units on the contour values are 10^{15} n/cm^2/s/sr/eV/s/MW.

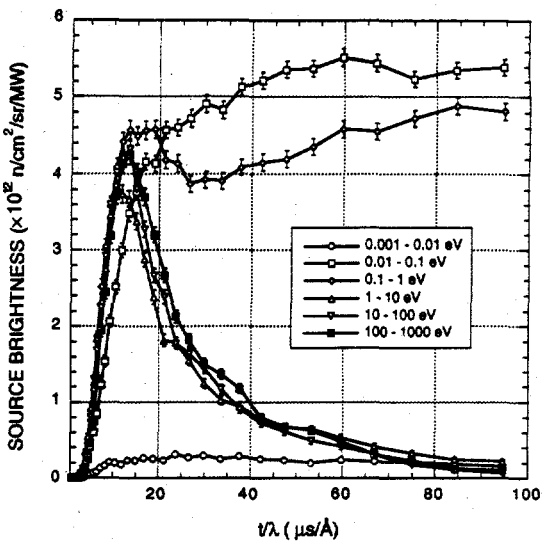

Figure 7. Reduced time spectrum for the 60-cm Be/Pb case.

3. Parameterization of the Source Brightness

The calculated brightness is used as a source term by the Monte Carlo instrument design code using the MCLIB library. Parameterization of time and energy dependence of the source brightness allows us to efficiently sample from a function describing the source distribution using simple random sampling.

The semi-empirical function used to characterize the source term is a Gaussian $G(t/\lambda)$ convolved with the sum of epithermal and thermal decay terms whose relative magnitudes are controlled by a switch function $S(\lambda)$:

$$I(t,\lambda) = G\left(\frac{t}{\lambda}\right) \otimes \left\{\left[1-S(\lambda)\right]\exp\left(-\frac{t/\lambda}{\eta}\right) + S(\lambda)\left[(1-R)\exp\left(-\frac{t}{\tau_1}\right) + R\exp\left(-\frac{t}{\tau_2}\right)\right]\right\}, \quad (1)$$

where

$$G\left(\frac{t}{\lambda}\right) \equiv \frac{1}{\sigma\sqrt{2\pi}}\exp\left\{-\frac{1}{2}\left[\frac{(t/\lambda)-\Delta}{\sigma}\right]^2\right\} \quad (2)$$

and

$$S(\lambda) = \exp\left(-\frac{\lambda_0}{\lambda}\right)^P. \quad (3)$$

There are eight fitting parameters in this function. The Gaussian $G(t/\lambda)$ is characterized by two parameters, the width σ and the delay Δ. The first term of the function with which the Gaussian is convolved describes the decay of the epithermal portion of the spectrum, where the "epithermal exponential" η defines the decay constant of epithermal neutrons. These three parameters, σ, Δ, and η, are determined by a least-squares fit to the reduced time spectrum over the range 1 μs/Å to 30 μs/Å. The parameters τ_1 and τ_2 are the long- and short-time decay

constants, respectively, on the tail of the thermal portion of the spectrum, while the ratio R defines the fraction of the tail populated by neutrons following the short-time decay. The switch function $S(\lambda)$ provides a smooth transition from an epithermal decay constant to a thermal decay constant. The switch function parameters λ_0 and P are determined by finding an appropriate value of the thermal/epithermal ratio at each of 18 wavelengths between 0.1 Å and 15 Å, and then least-squares fitting to these values (see also Figure 4 of ref. [2]).

Table 2 gives the values of the fitting parameters for the five reference cases. Note that, for all cases (except, perhaps, for the 60-cm Be/Pb case), only the thermal decay constants τ_1 and τ_2 vary appreciably, implying that the outer reflector size and material has a large effect on the tail of the thermal portion of the spectrum but only weakly impacts all other temporal characteristics.

Table 2. Fitting parameters for the five reference cases.

Case	τ_1 (μs)	τ_2 (μs)	R	η (μs/Å)	Δ (μs/Å)	σ (μs/Å)	λ_0 (Å)	P
40-cm Be/Ni	276	—	0	9.21	6.41	2.45	1.03	1.58
60-cm Be/Ni	414	—	0	9.24	6.40	2.34	0.90	1.81
40-cm Be/Pb	610	170	0.667	8.67	5.68	2.08	0.86	2.63
60-cm Be/Pb	734	170	0.4	7.37	3.32	3.32	1.2	0.6
150-cm Be	1710	380	0.6	8.96	6.45	2.54	0.77	2.3

5. Conclusion

We have characterized the temporal and energy dependence of the moderator brightness for five different reflector configurations for a flux-trap target system with four coupled liquid hydrogen moderators. An all-Be reflector yields the highest time-integrated low-energy brightness at the expense of very long tails. An outer reflector of Ni, which is a moderate thermal neutron absorber, exhibits very short tails. An outer reflector of Pb produces a higher peak brightness due to the additional neutron production derived from the Pb, while its low absorption cross section generates a high time-integrated brightness with only moderate tails.

6. Acknowledgements

This work was supported by the US. Department of Energy, BES-DMS, under Contract No. W-7405-Eng-36.

7. References

1. G. Russell, et al., "Coupled Moderator Neutronics," these proceedings.

2. P. Seeger, "The MCLIB Library: Monte Carlo Simulation of Neutron Scattering Instruments," these proceedings.

3. R. E. Prael, "A Review of Physics Models in the LAHET™ Code," Los Alamos National Laboratory report LA-UR-94-1817, and references cited therein.

4. T. O. Brun, et al., "LAHET Code System/CINDER'90 Validation Calculations and Comparison with Experimental Data," Proceedings of the Twelfth Meeting of the International Collaboration on Advanced Neutron Sources, ICANS-XII, Abingdon, U. K., 24-28 May, 1993, Rutherford Appleton Laboratory Report 94-025.

5. P. Ageron, Nucl. Instr. and Meth. **A284** (1989) 197.